Applied Physics A (2022) 128:926
https://doi.org/10.1007/s00339-022-06038-2

Applied Physics A
Materials Science & Processing

Graphitic carbon nitride–manganese oxide nanoflowers as promising T_1 magnetic resonance imaging contrast material

Zia Ur Rehman[1] · M. Zubair Iqbal[3] · Jianhua Hou[1] · Faheem K. Butt[2] · Salem AlFaify[4] · Bakhtiar Ul Haq[4] · Zeeshan Tariq[5] · Sajid Ur Rehman[5] · Muhammad Bilal[1] · Muhamamd Akram[2] · M. Umer Farooq[2]

Received: 10 March 2022 / Accepted: 7 September 2022 / Published online: 27 September 2022

Abstract

Hierarchical and flower-like nanostructures have attained great attention over the past decades due to their unique and intriguing properties. Considering the advantages of their particular structure and properties, we prepared g-C_3N_4/MnO_2 nanocomposite by microwave heating technique without using any catalysts, templates and organic reagents. The longitudinal and transverse relaxation time of as-synthesized nanocomposites were measured by using 0.55 T MRI instrument. Manganese is the primary origin for MRI and MR signals; therefore, different concentrations of the composite were dissolved in water. Relaxivities were measured by the inverse of relaxation times and plotted against the different concentrations of manganese. MRI results showed that the strength of the imaging signal is directly proportional to the Mn concentration, demonstrating that as-synthesized flower-like nanostructures have excellent T_1-weighted MRI performance. This study indicates that the nanocomposite of g-C_3N_4/MnO_2 could be a potential candidate as a bifunctional medical system that combines diagnostic imaging and targeted therapy.

✉ Jianhua Hou
jhhou@yzu.edu.cn

✉ Faheem K. Butt
faheemk.butt@ue.edu.pk

[1] School of Physics, College of Physical Science and Technology and School of Environmental Science and Engineering, Yangzhou University, Yangzhou 225000, China

[2] Department of Physics, Division of Science and Technology, University of Education Lahore, Lahore 54770, Pakistan

[3] School of Materials Science and Engineering, Zhejiang Sci-Tech University, Hangzhou, China

[4] Advanced Functional Materials and Optoelectronics Laboratory (AFMOL), Department of Physics, Faculty of Science, King Khalid University, P.O. Box 9004, Abha, Saudi Arabia

[5] School of Science, Optoelectronic Research Center, Minzu University of China, Beijing 100081, China

Graphical abstract

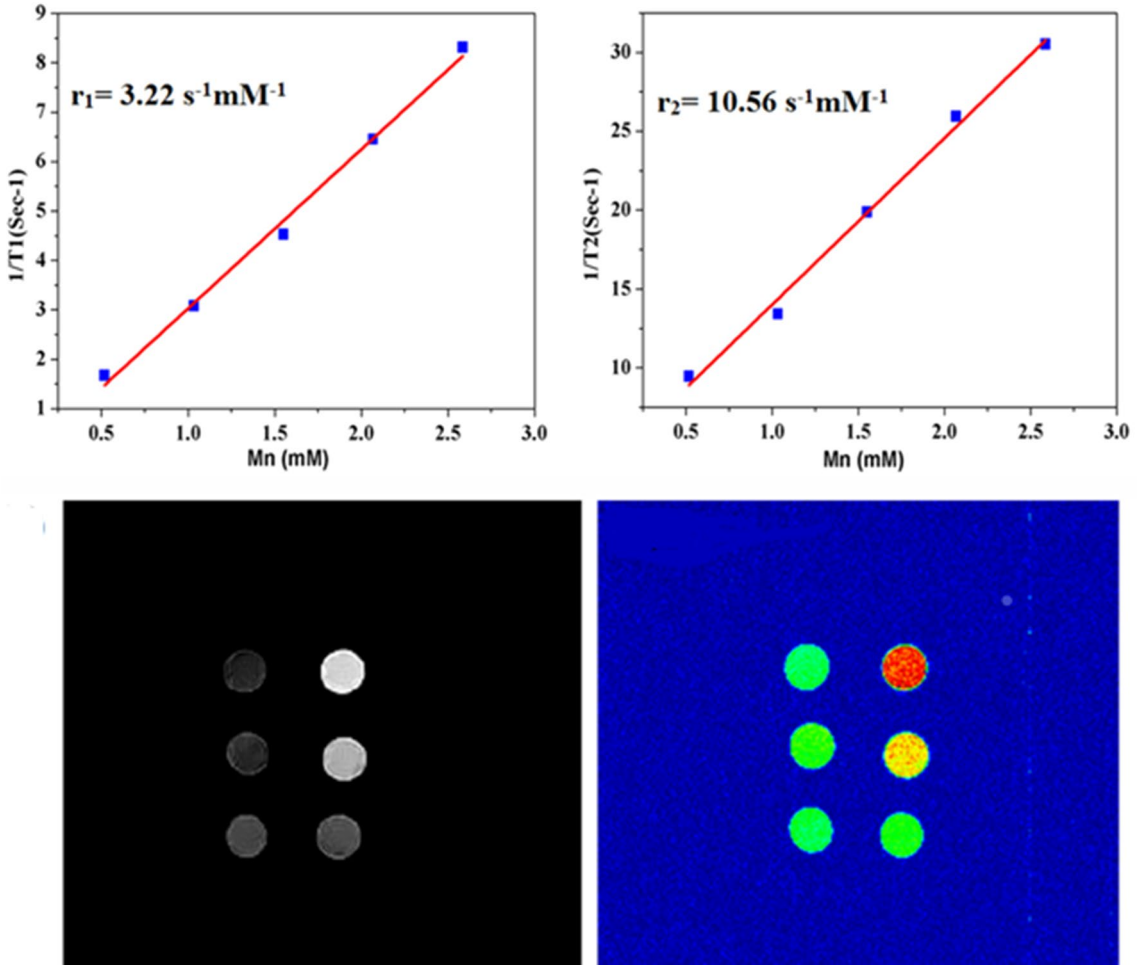

Keywords Graphitic carbon nitride · Nanoflowers · Magnetic resonance imaging · Contrast agent

1 Introduction

The utilization of synthesized and modified materials shows an upsurge due to their applications in various gadgets and smart devices. Various techniques have been designed to synthesize the desired structures for use in multiple applications, e.g., conversion of solar energy, fluorescence imaging and environmental purification [1–3]. g-C_3N_4 is abundant in nature and can be synthesized easily by using a one-step method involving the polymerization of less expensive precursors such as urea, [4, 5], dicyanamide [6, 7], thiourea [8, 9], cyanamide [10, 11], and melamine [12, 13]. Although the practical use of g-C_3N_4 is limited due to its smaller surface area and lower conductivity, its efficiency can be improved through structural engineering [14–17]. The structure of g-C_3N_4 contains 2D layers, which possess greater suitability for hybridization with other elements [18].

g-C_3N_4 and it nanocomposites have been used for many purposes, such as in photocatalysts, as fluorescent and gas sensors, as electrode of fuel cells and for hydrogen storage material [19, 20]. Wang et al. reported that g-C_3N_4 has a band gap 2.7 eV, which can be helpful to absorb light up to 460 nm. Polymer g-C_3N_4 is a novel and stable metal-free catalyst with high chemical and thermal stability and specific optical properties [21, 22]. Therefore, graphitic carbon nitride nanosheets are of great importance and have potential for additional biomedical and biological exploration [23]. Researchers from all over the world have reported g-C_3N_4-based nanocomposites such as graphitic-C_3N_4/metal oxides, graphitic-C_3N_4/inorganic acid salts composites, noble metal heterostructures of graphitic-C_3N_4 and graphitic-C_3N_4/halide heterojunctions by using different fabrication methods [18, 24, 25]. This work spurred significant interest in the fabrications,

modifications and uses of nanocomposites based on g-C_3N_4.

As manganese dioxide (MnO_2) has extraordinary properties such as large surface area, fast electron transfer rate, and good light absorption ability. It has been proposed as a promising fluorescence quencher using fluorescence sensing systems. [26, 27]. Manganese-based nanocomposite have attained great attention and play a significant role in purely T_1 weighted contrast agents in MR imaging to increase biocompatibility and transverse relation time. Mostly Mn-based contrast agents contain Mn^{+2} chelates and MnO nanoparticles. Mn^{+2} causes some complications when used as MRI contrast material, such as excretion from the body and brain problems, which may be cause of irregularities in the nervous system of the body [28]. MnO NPs may produce some problems leading to toxicity of the liver and spleen. This toxicity can be decreased with the help of surface modification with other biocompatible materials [29]. MnO_2 nanoparticles have become a good research topic due to their capability to reduce Mn^{4+} to Mn^{2+} in tumor microenvironments (TMEs) as a theranostic agent [30]. Mn_3O_4 nanoparticles as contrast agents for MRI have gained good consideration as a manganese (III) complex for practical use in clinics. The combination of photothermal therapy and chemotherapy has become a good tumor ablation mathedology with excellent results as compared to the previous conventional techniques [31].

In previous conventional methods, a large amount of healthy cells were affected along with cancer cells due to non-selective radiation and medication. Since previuos years, the nanocomposites have attained great attention in this treatment methodology and drug delivery process due to their good optical properties and biocompatibility [32, 33]. So the nanocomposites as contrast agents with hyperthermia agents can give good results for precise treatment [34], but it is a big challenge to make nanostructures with homogeneous surface morphology without changing the individual material properties. Gohar Ijaz et al. synthesized Au@Mn_3O_4 nanoflowers with homogeneous structure to overcome this issue with novel methodology. This magnetoplasmonic nanoflowers has good biocompatibility and good nanoplatforms regarding tumor ablation and diagnosis in vitro and in vivo without toxic effects [35].

During the past few years, cancer has become a growing disease and reason of the deaths of many people in the twentieth century [36]. Many therapies have been presented, but have limited results due to the different types of tumors [37]. In previous years in the field of nanomedicine, many nanomaterial-based therapies have been approved in clinics. Therapy-based treatments and diagnostic models have many advantages and overcome the problems of traditional methodologies and side effects [38]. This can be achieved by the fabrication of multifunctional and biocompatible materials with homogeneous surfaces, less toxic and controlled dimensions which is a big challenge [39].

Mn with several photosensitizers has been investigated with remarkable results that are helpful in magnetic resonance imaging and phototherapy of tumors [40]. In this aspect, TiO_2 with Mn has enhanced the properties which are useful in the field of T_1-MR imaging [41]. Asim Mushtaq et al. synthesized the Mn-doped TiO_2 rhombic nanocomposite by the hydrothermal technique which has homogeneous morphology, controlled dimensions and good biocompatibility. This rhombic nanocomposite has been characterized by different techniques and has good properties in MRI, cellular uptake and photothermal therapy [42]. Some magnetic materials such as Mn, gadolinium and NPs of iron have become promising contrast materials for MRI due to good magnetic properties and less toxicity [43].

Magnetic resonance imaging is a good and safe diagnostic technique as compared to traditional mathodologies. So there is a need of such materials as MRI contrast agents to enhance the precise diagnosis of disease at the early stage [44]. These contrast agents are divided in two categories (1) + ve contrast agent (2) –ve contrast agent, which are helpful for T_1-weighted and T_2-weighted MRI, respectively. So selecting a good contrast agent can increase the efficiency of synthesized material for the desired applications [45, 46]. Scientists are finding some excellent alternative of Gd by synthesizing different contrast agents that are more biocompatible and have fewer side effects such as nephrogenic systemic fibrosis for clinical practice [47]. Iron-based contrast agents have gained more attention than the above-mentioned magnetic contrast agents due to the less toxicity and good compatibility in the field of nanomedicine. In this aspect, Fe_3O_4–HAp is a good candidate for T_1-MR imaging, but it is a big task to make this material with homogeneous suface-controlled dimensions and theranostic applications [48]. In this research work, we made MnO_2/g-C_3N_4 nanocomposite for MRI contrast material. This nanocomposite has great importance in MRI because it has properties of both materials, less toxic and biocompatible. So this synthesized material can play a significant role to increase the efficiency of T_1-magnetic resonance imaging as contrast material.

g-C_3N_4/MnO_2 has shown applications in various fields such as biomedicine, energy storage devices, and biotechnology [23, 49]. g-C_3N_4/MnO_2 is also being used in cancer treatment as diagnostic material [23, 49]. Other fields involving the use of this composite material are in fiber and textile industries to remove the organic pollutants from wastewater [50]. Xiao-Long Zhang et al. [23] designed a novel fluorescence sensor based on g-C_3N_4 nanosheets along with a sandwich of MnO_2 composite, typically used for selective as well as quick sensing of glutathione living cells and aqueous solutions. They used a one-step easy redox method for fabrication of the nanocomposite material for the first time. Their findings showed that

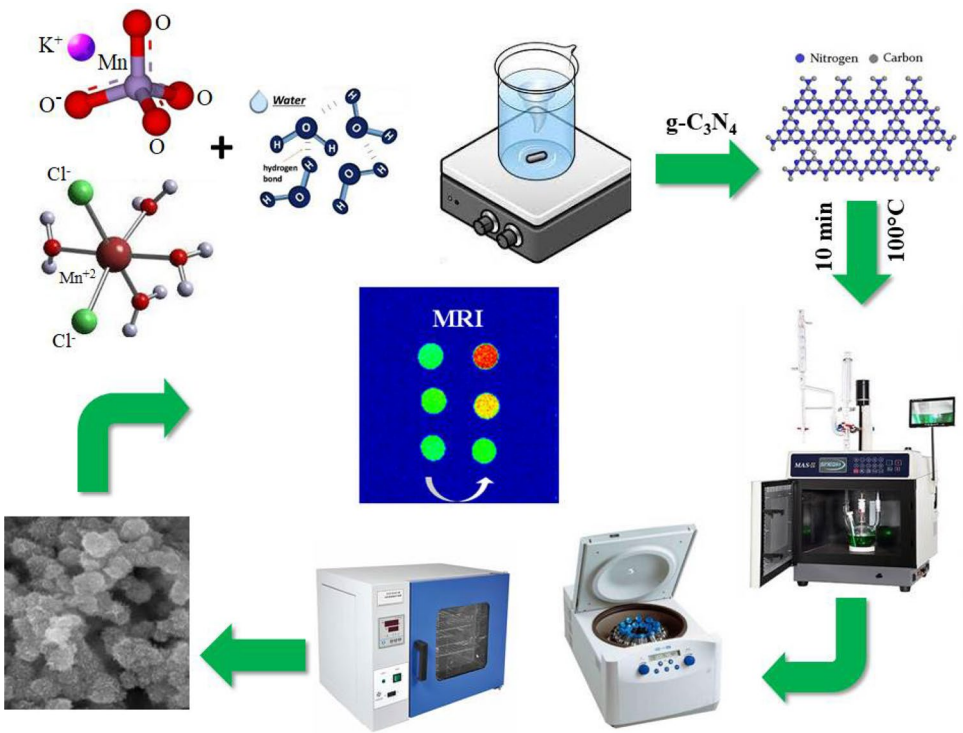

Scheme 1 Schematic representation of the synthesis process, surface modification and T_1 MR imaging by homogeneous MnO_2/g-C_3N_4 nanoflowers

the resultant nanocomposite has many characteristics such as turn-on fluorescence response, lower toxic levels, easy preparation and reduced cost. This nanoprobe of fluorescence can be prolonged to explain the biological roles of glutathione in the metabolism processes, cellular homeostasis and also in pathophysiological situations. Moreover, they showed that the as-synthesized nanocomposite has potential applications in the field of photoelectric and photocatalytic activities [23]. Their research also indicated the possible use of nanocomposite in fluorescence-related properties and exhibited its easy integration with other functional materials. Therefore, nanosheets of graphitic carbon nitride are of great importance and potential for additional biomedical and biological exploration [23].

Herein, we synthesized the effective nanocomposite by adding the high biocompatible materials MnO_2 and g-C_3N_4 via microwave-assisted method to increase the efficiency of T_1 magnetic resonance imaging. The method of preparing nanoflowers for MRI is given in Scheme 1.

We also discussed its possible use as promising MR imaging contrast material for the first time. These results showed that MnO_2/g-C_3N_4 nanocomposite has great potential as contrast MRI agent for diagnostic imaging and therapy of the affected area.

2 Experimental methods

2.1 Synthesis of graphitic carbon nitride (g-C_3N_4)

First, urea (15 g, Merck KgaA, extra pure) was taken in a ceramic crucible and placed in a muffle furnace for 3 h at 550 °C with a heating rate of 10° per min. Later on, it was permitted to cool down naturally to room temperature. g-C_3N_4 powder with light-yellow color was obtained.

2.2 Synthesis of MnO_2/g-C_3N_4 nanocomposite

For the synthesis of MnO_2/g-C_3N_4 nanostructures, 0.63 g of $KMnO_4$ and 1.18 g of $MnCl_2.4H_20$ were mixed in 100 ml water with constant magnetic stirring. After a few minutes, 0.1 g of g-C_3N_4 was added to the suspension and stirred continuously. The homogenous solution was poured into a 500 ml three-necked flask that was placed in a microwave oven attached to a water condenser for cooling. The temperature of the microwave oven was adjusted at 100 °C for heating the solution (10 min) at 700 W. After

the completion of the reaction, the solution was cooled down naturally and left for 1 day (24 h). The solution was centrifuged (12,000 rpm) several times for 4–5 min by using de-ionized water and ethanol as solvent. The precipitates were obtained and dried in a heating oven for 12 h at 90 °C.

3 Characterization

To check the structure and phase analysis of the prepared nanocomposites, X-ray diffractrometery (XRD) was used. SEM was done to analyze the surface formation of the prepared material. Raman spectroscopy was also used to study structural characterization.

3.1 MRI and relaxation characterization

Relaxivities (r_1 and r_2) and transverse and longitudinal relaxation times (T_1 and T_2) of nanocomposite material was measured with the help of a 0.55 T magnetic resonance imaging (MRI) device. For imaging and calculating the relaxation time T_1, the prepared nanoflowers were dissolved in solutions containing water with different concentrations of Mn (0.52, 1.03, 1.55, 2.06 and 2.58 mmol). Mn was used instead of carbon nitride in the prepared samples, because only Mn is the basic source in the MR signal and consequently in imaging. The different concentrations of Mn were obtained with the help of inductively coupled plasma mass spectrometry (ICP–MS). Longitudinal (r_1) and transverse (r_2) relaxivities were measured by taking the inverse of relaxation times ($1/T_1$, $1/T_2$) and plotted with various concentrations of Mn. Standard spin echo (SE) sequence was measured with parameters TR = 300 ms and TE = 18 ms with the help of the 0.55 T MRI device for T_1-weighted MR image.

4 Results and discussion

4.1 XRD analysis

The XRD pattern of MnO_2 is shown in Fig. 1a. The most prominent peak of pure MnO_2 corresponds to (211) and is matched with JCPDS card no. 44-0141 [51]. It is also confirmed through XRD pattern that only a single phase contains MnO_2. Figure 1a peaks also show the nanocrystal nature of MnO_2.

The XRD graph of the MnO_2/g-C_3N_4 nanocomposite is illustrated in Fig. 1b. This image showed that the peak relevant to g-C_3N_4 shown at 27.3° corresponds to (002) plane, and the remaining peaks are related to manganese dioxide (MnO_2). Generally, bulk g-C_3N_4 exhibits two peaks in the XRD spectrum at 13.1° and 27.3° corresponding to the (100)

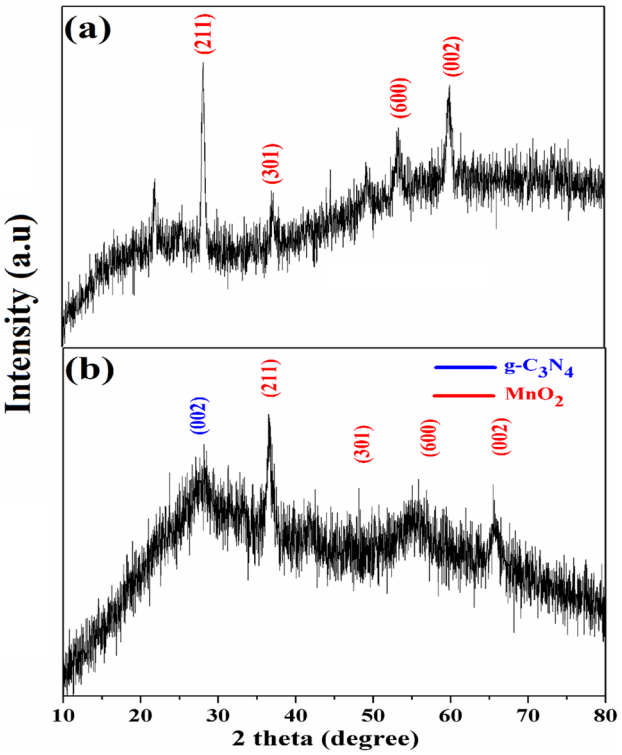

Fig. 1 XRD spectrum of **a** MnO_2 and **b** MnO_2/g-C_3N_4

and (002) planes. A dominant and clear peak can be seen at 27.3°, corresponding to *d*-spacing = 0.65 nm. There is a small shift between the bulk g-C_3N_4 and nanocomposite. The first peak of g-C_3N_4 did not appear in the XRD pattern and a small shift in the second peak is due to the composite with MnO_2. The other peaks in the XRD pattern represent the peaks of MnO_2 [51]. This nanocomposite XRD pattern proves the presence of both MnO_2 and g-C_3N_4 materials which may play an important role in MRI applications.

4.2 SEM analysis of MnO_2 and MnO_2/g-C_3N_4

The morphology of MnO_2 examined using scanning electron microscopy (SEM) is shown in Fig. 2. Figure 2a represents the SEM images at lower magnification (20 µm) and it is evident that the synthesized MnO_2 has hierarchical nanoflower structure.

The SEM image of MnO_2 resembles cotton flowers. Figure 2b shows the scanning electron microscopic image of MnO_2 at a higher resolution. Microspheres combine in the synthesis process and form nanoflowers. It also shows the surface to be a smooth, unique and homogeneous flower-like structure of MnO_2. The morphological study of MnO_2/g-C_3N_4 composite through SEM image Fig. 2c represents nonhomogenous and irregular surface. It is further observed that the morphology of nanocomposite material has rough surface with

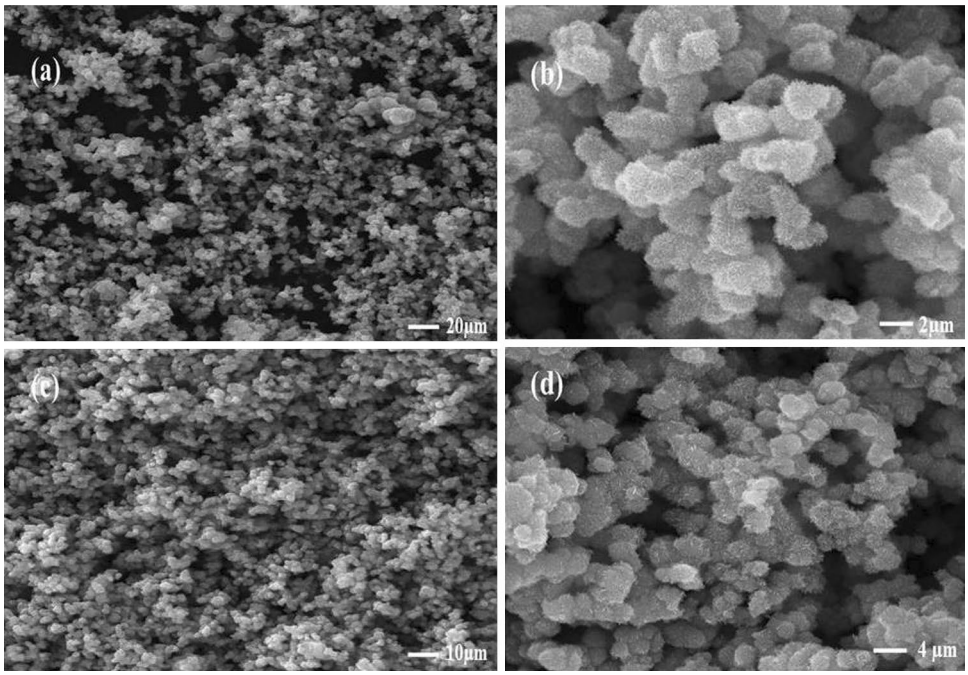

Fig. 2 SEM images of MnO_2 at **a** low resolution and **b** high resolution, **c** SEM images of MnO_2/g-C_3N_4 nanocomposite at lower resolution and **d** at higher resolution

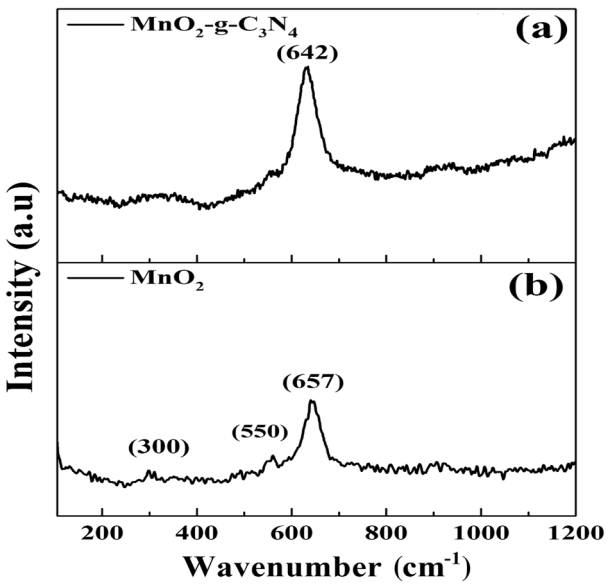

Fig. 3 Raman spectroscopy of **a** MnO_2/g-C_3N_4 and **b** MnO_2

large dense structure at 10 μm resolution. SEM analysis of the MnO_2/g-C_3N_4 nanocomposite presented in Fig. 2d indicates a cotton flower-like structure, large surface area and more active sties which may play a vital role in MRI applications.

4.3 Raman spectroscopic studies of MnO_2 and MnO_2/g-C_3N_4

Raman spectroscopic peak analysis of g-C_3N_4/MnO_2 nanocomposite and MnO_2 is displayed in Fig. 3a and b, respectively. Graph of Raman spectroscopy plotted between intensity (a.u) and wave number (cm^{-1}), as shown in Fig. 3a, manifests a broader peak at 642 cm^{-1} for MnO_2/g-C_3N_4 nanocomposite. The spectrum in Fig. 3b belongs to the β phase of MnO_2. Only one peak of β-MnO_2 was observed at 657 cm^{-1} in the Raman spectra. The other two peaks detected at 300 and 550 cm^{-1} are relatively smaller and belong to MnO_2 [52, 53]. Figure 3a further confirms that high-intensity peaks are observed for the MnO_2/g-C_3N_4 nanocomposite, showing that the material is crystalline [54, 55].

4.4 MRI and relaxation properties

T_1, T_2 relaxivities plots and T_1-weighted MR images of the nanostructure are shown in Fig. 4. The measurements were obtained by using different concentrations of Mn in an aqueous medium. In aqueous suspensions, the magnetic relaxivities of composite nanoflowers (CNFs) at room temperature were executed by applying a 0.55 T scanner. Associated with the contrast properties of the synthesized nanoflowers, the resultant quantitative data, i.e., the relaxivities values r_1 and r_2 are shown in Fig. 4a, b. The r_1 value is 3.22 $s^{-1}mM^{-1}$ and r_2 is 10.56 $s^{-1}mM^{-1}$, giving an r_2/r_1 ratio of 3.28, suggesting that the prepared nanopflowers are admirable T_1-weighted disparity representatives. MR imaging further confirmed the obtained quantitative data. A magnetic resonance imaging instrument (0.55 T) was used to investigate the enhancements of T_1-weighted MR signals. Compared to water, T_1-weighted MR images of CNFs are shown in Fig. 4c. MR imaging

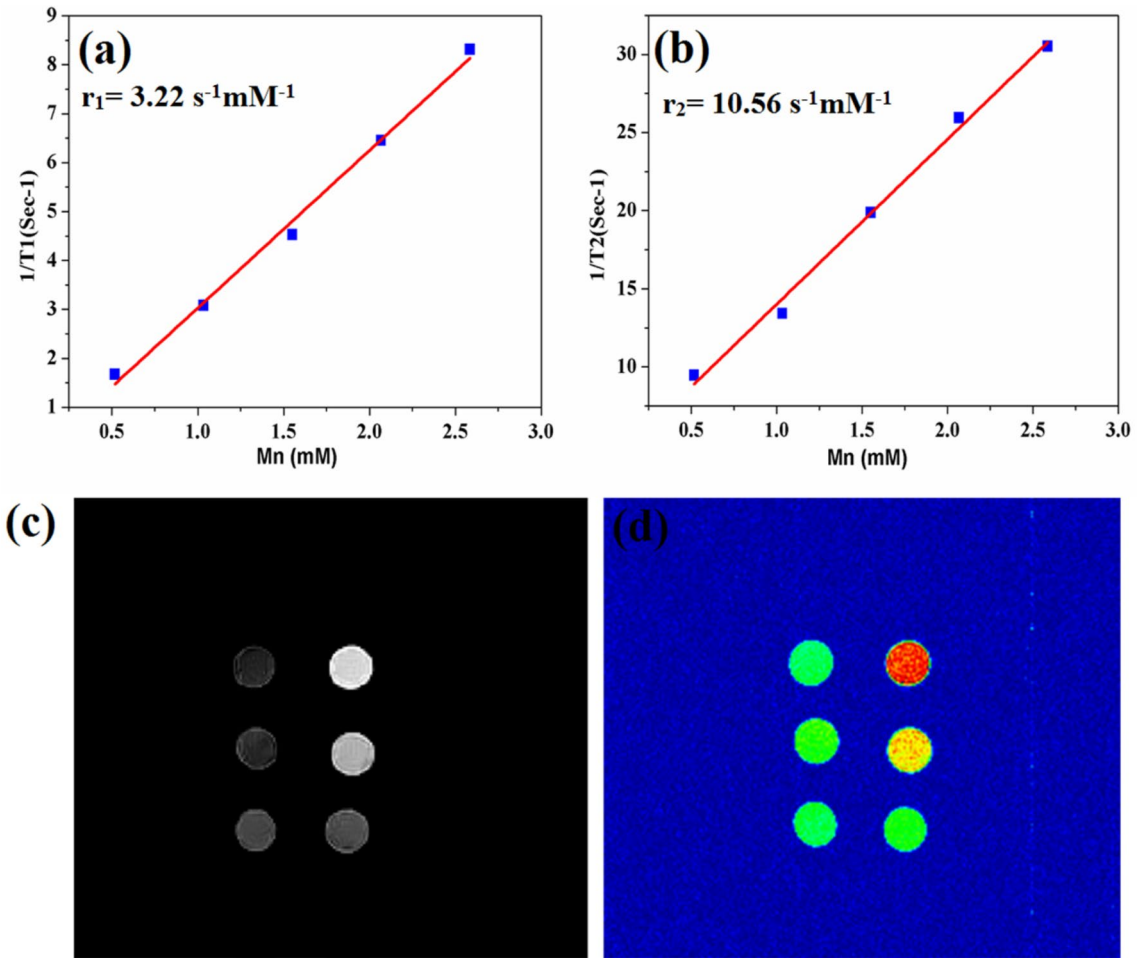

Fig. 4 **a, b** T_1, T_2 relaxivities plots. **c, d** T_1-weighted MR images of the nanostructure

results displayed that the intensity of the imaging signal was directly proportional to the concentration of Mn. On comparing with water, a sharp signal was detected for CNFs because of magnetic resonance imaging. The intensity of MRI signal can be distinguished in Fig. 4d. The T_1 and T_2 relaxation times, type of pulse sequence and method of *K*-space filling may affect the intensity of the MR image. The circles from dark to bright are present in the MRI images of the synthesized material. The dark areas represent the water and bright areas showing the Mn concentration. Initially, the signal intensity is low, so the images show prominent dark region, then the signal intensity becomes gradually increased and the bright areas in MRI image become more prominent due to the high concentration of Mn. Based on the above imaging results and MR relaxivities, it is inferred that the successfully prepared composite nanopflowers have excellent T_1-weighted MRI performance.

5 Conclusion

In this work we presented the synthesis of the g-C_3N_4 and MnO_2 composite nanoflowers by microwave-assisted technique. XRD results showed the peak of g-C_3N_4 at 27.3 °C, which confirms the presence of carbon nitride. From Raman spectra, it is clear that the composite material displays higher peak as compared to MnO_2. Furthermore, magnetic relaxivities were executed by applying a 0.55 T scanner with different concentrations of Mn at room temperature. The MRI results also displayed that the strength of imaging signal is directly proportional to the concentration of Mn and the prepared composite nanoflowers have excellent T_1-weighted MRI performance. These results show that the graphitic carbon nitride/MnO_2 composite nanoflowers can be used as MRI agent and in other biomedical applications.

Acknowledgements Faheem K. Butt and Zia Ur Rehman acknowledge the financial support from HEC Pakistan through grant number 7435/Punjab/NRPU/R&D/HEC/2017. J.H. Hou acknowledges the funding support from the National Natural Science Foundation of China (51602281), Yangzhou University High-end Talent Support Program and the "Qinglan Project" of Jiangsu Universities. The authors (S. AlFaify and B. Haq) extend their appreciation to the Deanship of Scientific Research at King Khalid University for funding this work through the Research Groups Program under Grant No. R.G.P. 2./21/40.

Funding Funding was provided by the Higher Education Commision, Pakistan, 7435/Punjab/NRPU/R&D/HEC/2017 to Faheem khurshid Butt; National Natural Science Foundation of China, 51602281 to Jianhua Hou; and King Khalid University, R.G.P. 2./21/40 to Salem Alfaify.

Availability of data and material Not applicable.

Code availability Not applicable.

Declarations

Conflict of interest None of the authors have any financial or competing interests that would have appeared to influence the work reported in this paper.

Ethical approval Not applicable.

Consent to participate Not applicable.

Consent for publication Not applicable.

References

1. W. Guo et al., Direct growth of TiO_2 nanosheet arrays on carbon fibers for highly efficient photocatalytic degradation of methyl orange. Adv. Mater. **24**(35), 4761–4764 (2012)
2. Z.-M. Yang et al., Novel Ag_3PO_4/CeO_2 composite with high efficiency and stability for photocatalytic applications. J. Mater. Chem. A **2**(6), 1750–1756 (2014)
3. L.-R. Zou et al., A facile and rapid route for synthesis of gC_3N_4 nanosheets with high adsorption capacity and photocatalytic activity. RSC Adv. **6**(89), 86688–86694 (2016)
4. B. Chai et al., Graphitic carbon nitride (gC_3N_4)–Pt-TiO_2 nanocomposite as an efficient photocatalyst for hydrogen production under visible light irradiation. Phys. Chem. Chem. Phys. **14**(48), 16745–16752 (2012)
5. F. Dong et al., Efficient synthesis of polymeric gC_3N_4 layered materials as novel efficient visible light driven photocatalysts. J. Mater. Chem. **21**(39), 15171–15174 (2011)
6. G. Zhang et al., Polycondensation of thiourea into carbon nitride semiconductors as visible light photocatalysts. J. Mater. Chem. **22**(16), 8083–8091 (2012)
7. J. Zhang et al., A facile band alignment of polymeric carbon nitride semiconductors to construct isotype heterojunctions. Angew. Chem. Int. Ed. **51**(40), 10145–10149 (2012)
8. J. Hong et al., Mesoporous carbon nitride with in situ sulfur doping for enhanced photocatalytic hydrogen evolution from water under visible light. J. Mater. Chem. **22**(30), 15006–15012 (2012)
9. Y. Zhang et al., Porous graphitic carbon nitride synthesized via direct polymerization of urea for efficient sunlight-driven photocatalytic hydrogen production. Nanoscale **4**(17), 5300–5303 (2012)
10. K. Takanabe et al., Photocatalytic hydrogen evolution on dye-sensitized mesoporous carbon nitride photocatalyst with magnesium phthalocyanine. Phys. Chem. Chem. Phys. **12**(40), 13020–13025 (2010)
11. X. Wang et al., A metal-free polymeric photocatalyst for hydrogen production from water under visible light. Nat. Mater. **8**(1), 76–80 (2009)
12. Y. Wang et al., Graphite-like C_3N_4 hybridized $ZnWO_4$ nanorods: synthesis and its enhanced photocatalysis in visible light. CrystEngComm **14**(15), 5065–5070 (2012)
13. S. Yan, Z. Li, Z. Zou, Photodegradation of rhodamine B and methyl orange over boron-doped g-C_3N_4 under visible light irradiation. Langmuir **26**(6), 3894–3901 (2010)
14. Y. Cui et al., Synthesis of bulk and nanoporous carbon nitride polymers from ammonium thiocyanate for photocatalytic hydrogen evolution. J. Mater. Chem. **21**(34), 13032–13039 (2011)
15. Z.-F. Huang et al., Carbon nitride with simultaneous porous network and O-doping for efficient solar-energy-driven hydrogen evolution. Nano Energy **12**, 646–656 (2015)
16. J. Qin et al., Improving the photocatalytic hydrogen production of Ag/gC_3N_4 nanocomposites by dye-sensitization under visible light irradiation. Nanoscale **8**(4), 2249–2259 (2016)
17. Z. Yang, Y. Zhang, Z. Schnepp, Soft and hard templating of graphitic carbon nitride. J. Mater. Chem. A **3**(27), 14081–14092 (2015)
18. Z. Zhao, Y. Sun, F. Dong, Graphitic carbon nitride based nanocomposites: a review. Nanoscale **7**(1), 15–37 (2015)
19. M. Tahir et al., Tubular graphitic-C_3N_4: a prospective material for energy storage and green photocatalysis. J. Mater. Chem. A **1**(44), 13949–13955 (2013)
20. M. Tahir et al., Large scale production of novel g-C_3N_4 micro strings with high surface area and versatile photodegradation ability. CrystEngComm **16**(9), 1825–1830 (2014)
21. X. Wang et al., Polymer semiconductors for artificial photosynthesis: hydrogen evolution by mesoporous graphitic carbon nitride with visible light. J. Am. Chem. Soc. **131**(5), 1680–1681 (2009)
22. Y. Wang, X. Wang, M. Antonietti, Polymeric graphitic carbon nitride as a heterogeneous organocatalyst: from photochemistry to multipurpose catalysis to sustainable chemistry. Angew. Chem. Int. Ed. **51**(1), 68–89 (2012)
23. X.-L. Zhang et al., Turn-on fluorescence sensor for intracellular imaging of glutathione using g-C_3N_4 nanosheet–MnO_2 sandwich nanocomposite. Anal. Chem. **86**(7), 3426–3434 (2014)
24. F.K. Butt et al., Synthesis of novel ZnV_2O_4 spinel oxide nanosheets and their hydrogen storage properties. CrystEngComm **16**(5), 894–899 (2014)
25. F.K. Butt et al., Fabrication of ZnV_2O_6 nanostructures: their energy storage and PL properties. Mater. Lett. **155**, 15–17 (2015)
26. R. Deng et al., Intracellular glutathione detection using MnO_2-nanosheet-modified upconversion nanoparticles. J. Am. Chem. Soc. **133**(50), 20168–20171 (2011)
27. Y. Wang et al., A FRET-based carbon dot–MnO2 nanosheet architecture for glutathione sensing in human whole blood samples. Chem. Commun. **51**(64), 12748–12751 (2015)
28. V.A. Fitsanakis et al., The use of magnetic resonance imaging (MRI) in the study of manganese neurotoxicity. Neuro Toxicol. **27**(5), 798–806 (2006)
29. Q. Wu et al., MnO2-laden black phosphorus for MRI-guided synergistic PDT PTT, and chemotherapy. Matter **1**(2), 496–512 (2019)
30. M. Zhang et al., Tumor environment responsive degradable CuS@ $mSiO_2$@ MnO_2/DOX for MRI guided synergistic chemo-photothermal therapy and chemodynamic therapy. Chem. Eng. J **389**, 124450 (2020)

31. V. Peruzzo, S. Tamburini, P.A. Vigato, Manganese complexes with planar or tridimensional acyclic or cyclic Schiff base ligands. Inorg. Chim. Acta **387**, 151–162 (2012)
32. M. Li et al., Au@ MnS@ ZnS core/shell/shell nanoparticles for magnetic resonance imaging and enhanced cancer radiation therapy. ACS Appl. Mater. Interfaces **8**(15), 9557–9564 (2016)
33. W. Chen et al., Structural-engineering rationales of gold nanoparticles for cancer theranostics. Adv. Mater. **28**(39), 8567–8585 (2016)
34. K. Yang et al., Multimodal imaging guided photothermal therapy using functionalized graphene nanosheets anchored with magnetic nanoparticles. Adv. Mater. **24**(14), 1868–1872 (2012)
35. G.I. Dar et al., Facile synthesis of Au@ Mn_3O_4 magneto-plasmonic nanoflowers for T_1-weighted magnetic resonance imaging and photothermal therapy of cancer. J. Mater. Chem. B **8**(36), 8356–8367 (2020)
36. J. Shi et al., Cancer nanomedicine: progress, challenges and opportunities. Nat. Rev. Cancer **17**(1), 20–37 (2017)
37. N. McGranahan, C. Swanton, Clonal heterogeneity and tumor evolution: past, present, and the future. Cell **168**(4), 613–628 (2017)
38. N. Ahmed, H. Fessi, A. Elaissari, Theranostic applications of nanoparticles in cancer. Drug Discov. Today **17**(17–18), 928–934 (2012)
39. A. Solanki, J.D. Kim, K.-B. Lee, Nanotechnology for regenerative medicine: nanomaterials for stem cell imaging. Nanomedicine **3**(4), 567–578 (2008)
40. F. Wu et al., A Simple Strategy to Fabricate Phthalocyanine-Encapsulated Nanodots for Magnetic Resonance Imaging and Antitumor Phototherapy. ACS Appl. Bio. Mater. **3**(6), 3681–3689 (2020)
41. M.Z. Iqbal et al., Silica-coated super-paramagnetic iron oxide nanoparticles (SPIONPs): a new type contrast agent of *T*1 magnetic resonance imaging (MRI). J. Mater. Chem. B **3**(26), 5172–5181 (2015)
42. A. Mushtaq et al., Facile synthesis of Mn doped TiO_2 rhombic nanocomposites for enhanced *T*1-Magnetic resonance imaging and photodynamic therapy. Mater. Res. Bull. **144**, 111481 (2021)
43. D. Shen, G. Wu, H.-I.I. Suk, Deep learning in medical image analysis. Annu. Rev. Biomed. Eng. **19**, 221 (2017)
44. K.R. Thiim et al., Clinical experience with an in-NICU magnetic resonance imaging system. J. Perinatol. **42**(7), 873–879 (2022)
45. A. Koudrina et al., Exploring the unique contrast properties of aptamer-gadolinium conjugates in magnetic resonance imaging for targeted imaging of thrombi. ACS Appl. Mater. Interfaces **13**(8), 9412–9424 (2021)
46. M.F. Tweedle, Alternatives to gadolinium-based contrast agents. Invest. Radiol. **56**(1), 35–41 (2021)
47. P. Boehm-Sturm et al., Low-molecular-weight iron chelates may be an alternative to gadolinium-based contrast agents for *T*1-weighted contrast-enhanced MR imaging. Radiology **286**(2), 537–546 (2018)
48. V. Zheltova et al., Fe_3O_4@ HAp core–shell nanoparticles as MRI contrast agent: Synthesis, characterization and theoretical and experimental study of shell impact on magnetic properties. Appl. Surf. Sci. **531**, 147352 (2020)
49. M. Wu et al., Manganese dioxide nanosheets: from preparation to biomedical applications. Int. J. Nanomed. **14**, 4781 (2019)
50. M. Wang et al., 2D–2D MnO_2/g-C_3N_4 heterojunction photocatalyst: in-situ synthesis and enhanced CO_2 reduction activity. Carbon **120**, 23–31 (2017)
51. S. Devaraj, N. Munichandraiah, Effect of crystallographic structure of MnO_2 on its electrochemical capacitance properties. J. Phys. Chem. C **112**(11), 4406–4417 (2008)
52. Z. Ali et al., Effect of synthesis technique on electrochemical performance of bismuth selenide. J. Power Sources **229**, 216–222 (2013)
53. M. Tahir et al., Bifunctional catalysts of Co_3O_4@ GCN tubular nanostructured (TNS) hybrids for oxygen and hydrogen evolution reactions. Nano Res. **8**(11), 3725–3736 (2015)
54. F.K. Butt et al., Synthesis of novel ZnV_2O_4 hierarchical nanospheres and their applications as electrochemical supercapacitor and hydrogen storage material. ACS Appl. Mater. Interfaces **6**(16), 13635–13641 (2014)
55. J. Li et al., Architecture of PtFe/C catalyst with high activity and durability for oxygen reduction reaction. Nano Res. **7**(10), 1519–1527 (2014)

Terms and Conditions

Springer Nature journal content, brought to you courtesy of Springer Nature Customer Service Center GmbH (“Springer Nature”).
Springer Nature supports a reasonable amount of sharing of research papers by authors, subscribers and authorised users (“Users”), for small-scale personal, non-commercial use provided that all copyright, trade and service marks and other proprietary notices are maintained. By accessing, sharing, receiving or otherwise using the Springer Nature journal content you agree to these terms of use (“Terms”). For these purposes, Springer Nature considers academic use (by researchers and students) to be non-commercial.
These Terms are supplementary and will apply in addition to any applicable website terms and conditions, a relevant site licence or a personal subscription. These Terms will prevail over any conflict or ambiguity with regards to the relevant terms, a site licence or a personal subscription (to the extent of the conflict or ambiguity only). For Creative Commons-licensed articles, the terms of the Creative Commons license used will apply.
We collect and use personal data to provide access to the Springer Nature journal content. We may also use these personal data internally within ResearchGate and Springer Nature and as agreed share it, in an anonymised way, for purposes of tracking, analysis and reporting. We will not otherwise disclose your personal data outside the ResearchGate or the Springer Nature group of companies unless we have your permission as detailed in the Privacy Policy.
While Users may use the Springer Nature journal content for small scale, personal non-commercial use, it is important to note that Users may not:

1. use such content for the purpose of providing other users with access on a regular or large scale basis or as a means to circumvent access control;
2. use such content where to do so would be considered a criminal or statutory offence in any jurisdiction, or gives rise to civil liability, or is otherwise unlawful;
3. falsely or misleadingly imply or suggest endorsement, approval , sponsorship, or association unless explicitly agreed to by Springer Nature in writing;
4. use bots or other automated methods to access the content or redirect messages
5. override any security feature or exclusionary protocol; or
6. share the content in order to create substitute for Springer Nature products or services or a systematic database of Springer Nature journal content.

In line with the restriction against commercial use, Springer Nature does not permit the creation of a product or service that creates revenue, royalties, rent or income from our content or its inclusion as part of a paid for service or for other commercial gain. Springer Nature journal content cannot be used for inter-library loans and librarians may not upload Springer Nature journal content on a large scale into their, or any other, institutional repository.
These terms of use are reviewed regularly and may be amended at any time. Springer Nature is not obligated to publish any information or content on this website and may remove it or features or functionality at our sole discretion, at any time with or without notice. Springer Nature may revoke this licence to you at any time and remove access to any copies of the Springer Nature journal content which have been saved.
To the fullest extent permitted by law, Springer Nature makes no warranties, representations or guarantees to Users, either express or implied with respect to the Springer nature journal content and all parties disclaim and waive any implied warranties or warranties imposed by law, including merchantability or fitness for any particular purpose.
Please note that these rights do not automatically extend to content, data or other material published by Springer Nature that may be licensed from third parties.
If you would like to use or distribute our Springer Nature journal content to a wider audience or on a regular basis or in any other manner not expressly permitted by these Terms, please contact Springer Nature at

onlineservice@springernature.com